Apatite weathering as a geological driver of high uranium concentrations in groundwater

Andre Banning[a]*[1], Thomas R. Rüde[a]

[a]RWTH Aachen University, Institute of Hydrogeology, Lochnerstraße 4-20, 52064 Aachen, Germany.

*Corresponding author: email: andre.banning@rub.de; Tel.: +49-(0)234-32-23298

[1]Present address: Ruhr-Universität Bochum, Hydrogeology Department, Universitätsstraße 150, 44801 Bochum, Germany.

Abstract

Uranium is a heavy metal with potential adverse human health effects when consumed via drinking water. Although associated quality regulations have been implemented, geological sources and hydrogeochemical behavior of uranium in groundwater used for drinking water supply remain little understood. This study presents a hydrogeochemical and mineralogical characterization of a Triassic sandstone aquifer on a macro- and micro-scale, and an evaluation of uranium remobilization into groundwater, also considering the paleoenvironment and the distribution of the affected aquifer itself. Syndiagenetic uraniferous carbonate fluorapatite inclusions within the aquifer sandstones ("active arkoses") were found to show structurally (chemical substitution in the crystal structure) and radiatively (α-recoil damage from uranium decay) enhanced mineral solubility. Extraction experiments indicated that these inclusions release uranium to groundwater during weathering. In conclusion, apatite alteration was identified as the responsible mechanism for widespread groundwater uranium concentrations >10 µg L^{-1} in the region representing Germany´s most significant problem area in this respect. Therefore, results indicate that the studied sedimentary apatite deposits cause the regional geogenic groundwater uranium problem, and must be considered as potential uranium sources in comparable areas worldwide.

1 Introduction

1.1 Rationale

Uranium (U) is known to be a heavy metal with a nephrotoxic potential, possibly leading to adverse human health effects (Zamora et al., 1998; Kurttio et al., 2006). In order to limit public U exposure via drinking water, German authorities established a threshold value of 10 µg L^{-1} in 2011, making Germany the only European Union member state to date with a binding legislation in this respect. Sources of U in groundwater can be natural or anthropogenic. While the former is mostly represented by uraniferous rocks like felsic magmatites (Banning et al., 2012; Frengsted et al., 2000) or fen peats (Read et al., 1993; Banning et al., 2013), the latter includes former U mining sites (Carvalho et al., 2005; Baborowski and Bozau, 2006), depleted U ammunition (Crançon et al., 2010; Dong et al., 2006) or phosphorus fertilizer (Zielinski et al., 2006; Schnug and Lottermoser, 2013). Drinking water supply in northern Bavaria is dependent on groundwater extraction from terrestrial Triassic (Keuper) sandstones. Therein, large areas with groundwater U concentrations >10 µg L^{-1} were detected, making the region Germany´s most significant U problem area known so far. The U sources and mobilization processes have been unknown. Consequently, in an effort to unravel U dynamics in the given area, this study focused on a geochemical and mineralogical characterization of aquifer materials, elemental distribution on different scales, and U mineralogical fractionation and mobility.

1.2 Study area and "active arkoses"

The study area around the city of Nürnberg in southeastern Germany (Fig. 1,3) is part of the epicontinental South German Keuper Basin filled with terrestrial and shallow marine sediments (see geological map, Fig. A1 in the Appendix). A medium to coarse grained, feldspathic sandstone ("Burgsandstein", Fig. 2) with clayey interbeddings from the terrestrial facies represents the major aquifer used for water extraction in the region.

Typical groundwater type in the "Burgsandstein" aquifer is Ca-Mg-HCO_3 (Heinrichs and Udluft, 1999). Hydrochemical data for 21 groundwater samples from this aquifer (kindly provided by the Bavarian Environment Agency, LfU) indicates a circumneutral pH milieu (mean: 7.1, ranging from 5.2-8.3). pH does not show any correlation with U concentrations (R^2=0.04), maximum values are found around pH 7. The same is valid for U correlation with NO_3^- (R^2=0.10) or eC (R^2=0.02). Total organic carbon is <0.1 mg L^{-1} in most groundwaters including all samples with U>10 µg L^{-1}. Uranium concentrations above the guideline value were only found in oxic waters with Fe and Mn below detection limits and NO_3^- presence, while anoxic waters containing Fe and Mn (but no nitrate) yielded low U. These observations reflect the redox-dependent mobility of U in solution being mobile as U(VI) and insoluble as U(IV).

The sandstone contains abundant U-rich intercalations appearing in outcrops as mainly red to violet lenses, shards or cloudy patches with partly significant dimensions in the m^2 range.

These U anomalies were first discovered in the 1950s during U exploration programmes, but never mined due to their patchy distribution in the sandstone (Abele et al., 1962).

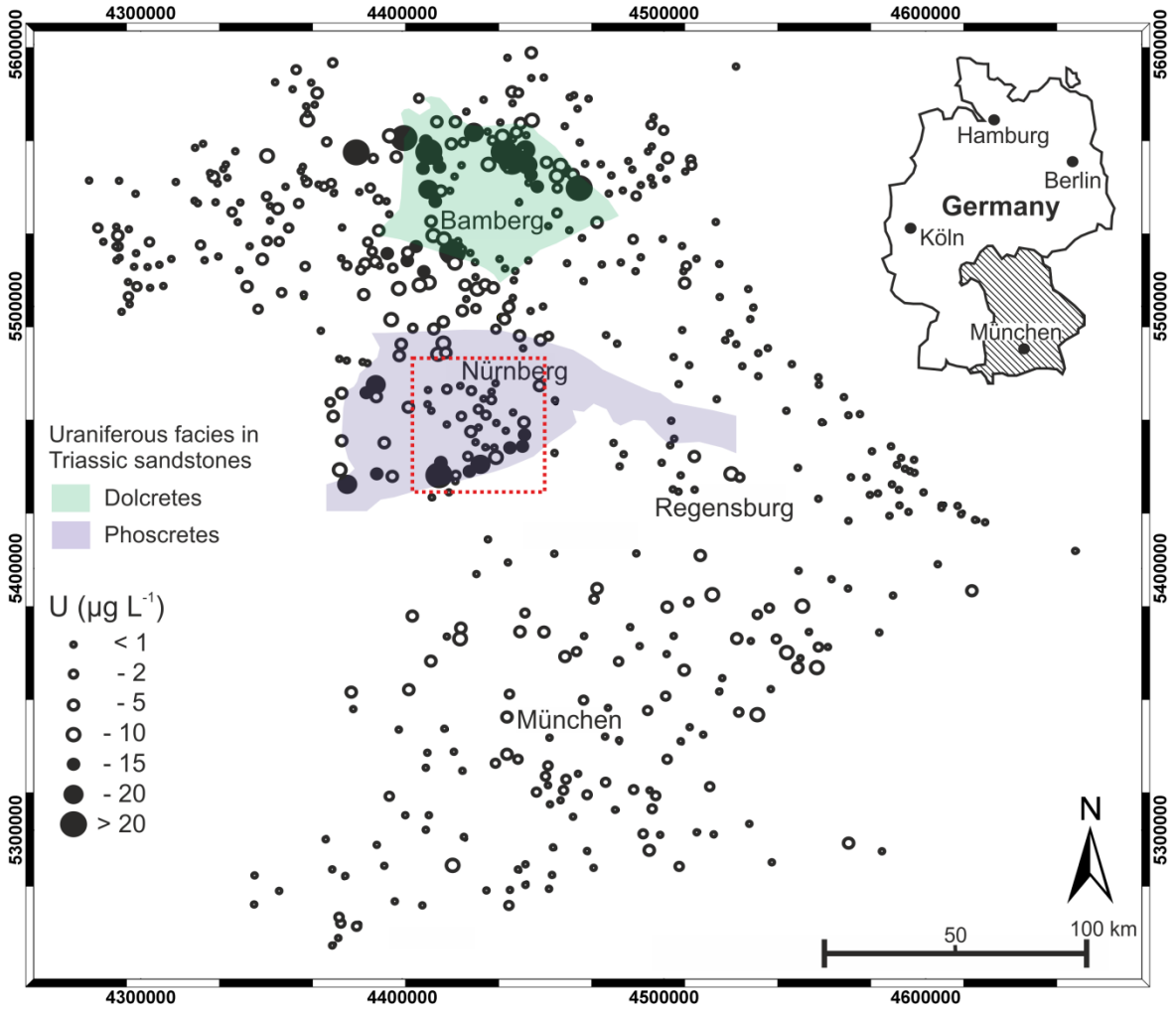

Fig. 1. Uranium concentrations in Bavarian drinking water and distribution of uraniferous facies in Triassic sandstones (the latter after Dill, 1988). The dashed red box indicates the study area.

Two main types of uraniferous sediments (also referred to as "active arkoses" due to significant radioactivity from U α-decay) were distinguished according to their paleogeographical position in the basin: carbonatic "dolcretes" in the northern, basinward part (playa margin, U bound to carbonate phases), and apatitic "phoscretes" (U bound to phosphate phases) deposited in a more proximal part of the sedimentary fan derived from Variscan provenance in the south (Dill, 1988; Figs. 1,3). This study focuses on the apatitic deposits. Carbonate fluorapatite (francolite) occurring as fine grained cement between the silicate grains was suggested as the U carrier phase (Abele et al., 1962). The heavy metal´s ability to substitute on the Ca site in the apatite crystal structure is explainable by the

similarity of U(IV) and Ca(II) ionic radii and can result in U contents up to the wt.% range (Starinsky et al., 1982; Rakovan et al., 2002).

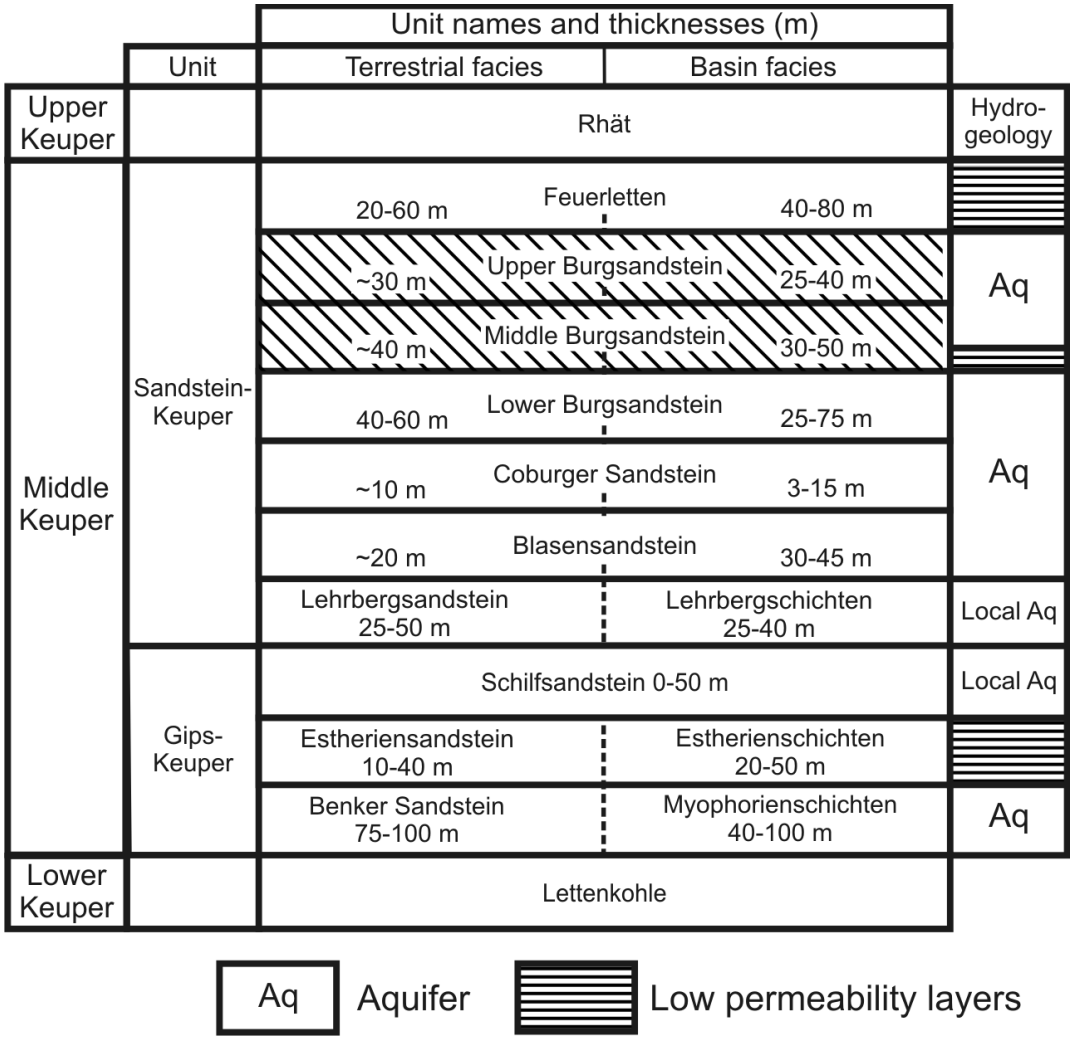

Fig. 2. Keuper stratigraphy of the study area with sampled units highlighted by hachures, approximate unit thicknesses and basic hydrogeology (modified after Heinrichs and Udluft, 1999). "Active arkoses" only occur in Middle and Upper "Burgsandstein" aquifers, parts of the terrestrial Norian "Sandsteinkeuper".

"Active arkoses" are interpreted as syndiagenetic formations derived from apatite precipitation from U-, Fe- and PO_4^{3-}-enriched groundwater with simultaneous immobilization of U. Precipitation of fine-grained apatite and ferric oxide occurred during a substantial rise of pH when the solution encountered playa lake carbonates. The apatites replaced the latter and therefore resemble the paleo distribution of Triassic playa lakes in the study area (Abele et al., 1962; Dill, 1988; Dill, 2010). These genetic and mineralogical aspects make the described German francolite occurrence readily comparable to numerous examples worldwide, e.g. in the U.S.A., Morocco, New Zealand, Sri Lanka and South

Africa (Swirydczuk et al., 1981; McArthur, 1985; Dahanayake and Subasinghe, 1989). Conclusions from these regions can be utilised in understanding this system, and vice versa, results on U dynamics obtained here may be transferred to comparable study areas.

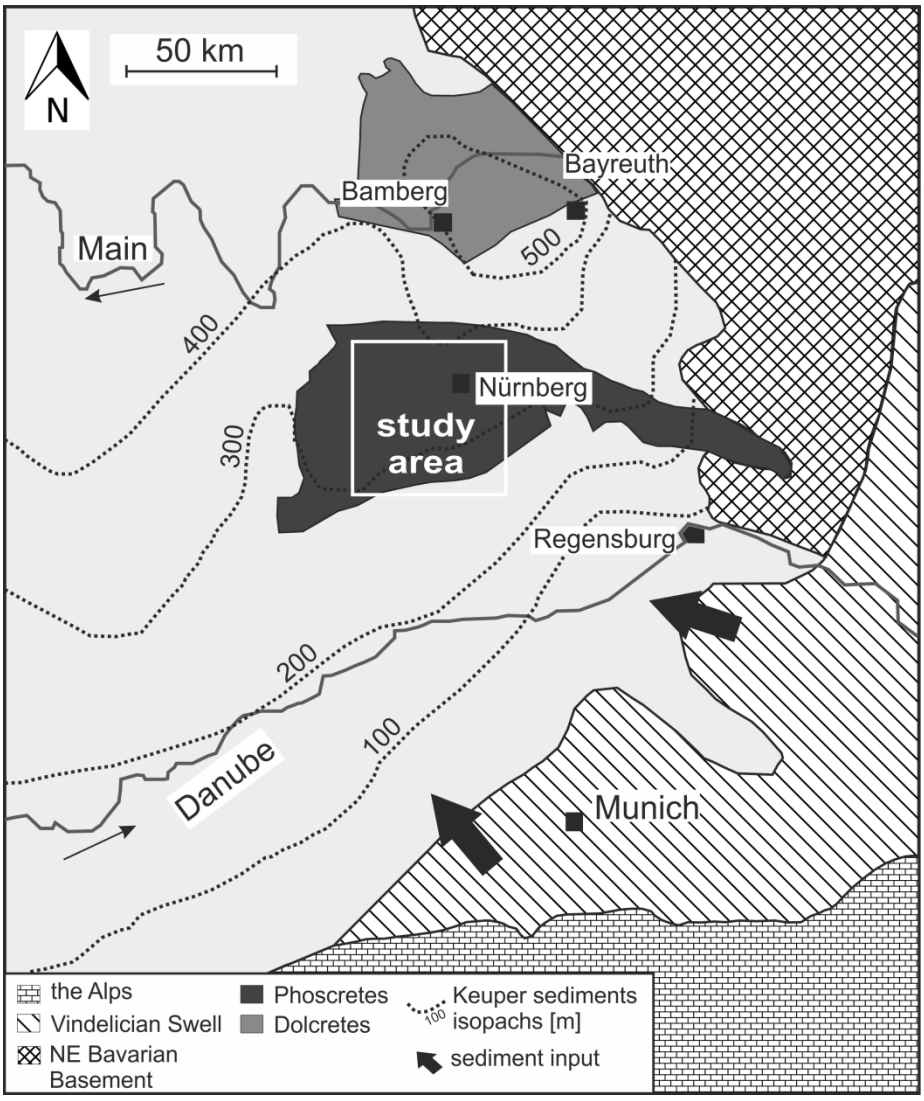

Fig. 3. Paleogeographical situation during the Middle Keuper with sediment input directions, sediment thicknesses and distribution of the main U-bearing depositional facies (modified after Dill, 1988; Dill 2010). See Fig. 1 for a geographical overview. The sedimentary basin filling mainly derived from erosion of the Vindelician Swell – a former part of the Central European Variscides consisting of crystalline magmatic and metamorphic rocks – under arid conditions. It may be subdivided into a terrestrial (alluvial fan with playa lakes) and a basinal (shallow marine) facies with transitional character (sabhka) in between (Abele et al., 1962; Dill, 2010; Heinrichs and Udluft, 1999).

2 Methodology

2.1 Hydrochemical data

A dissolved U distribution map for Bavarian drinking water (Fig. 1) was derived using freely available data from an internet resource provided by the German non-profit organisation "foodwatch" which collected and published U concentration data from Bavarian health and environmental authorities (Foodwatch, 2008). The dataset includes 703 single values obtained between 2000 and 2006. Drinking water U concentrations have partly decreased since then, mainly because of remediation measures taken by water suppliers as a reaction towards the political discussion on U limitations. Nevertheless, the map reflects the U occurrence in Bavarian groundwater (by far the most important drinking water source) during the given period. This approach – drawing conclusions from tap water quality to groundwater composition – is possible because of the special structure of drinking water supply in Bavaria: the highly decentralized system consists of around 2,350 municipal water suppliers enabling a spatially accurate and high-resolution visualization of U distribution.

2.2 Rock samples

A total of 47 rock samples were obtained from outcrops of the middle and upper Burgsandstein (Fig. 2, sampling locations in Fig. A1 in the Appendix). All samples were analyzed using INAA (thermal neutron flux: $7*10^{12}$ n cm^{-2} s^{-1}; Ge detector: resolution better than 1.7 keV for the 1332 keV, ^{60}Co photopeak) and total digestion ($HClO_4$-HNO_3-HCl-HF at 240°C) followed by ICP-OES analysis (Varian 735ES) for bulk rock geochemistry (49 elements, see complete data table A2 in the Appendix).

Ten samples (seven "active arkoses", two sandstones and one clay band) were selected for XRD analysis to characterize their mineralogical composition. These were ground to powder grain size in a McCrone corundum mill before measurements applying a Huber Co-kα diffractometer (operational adjustments: 40 kV, 40 mA; 2θ range: 2-110°, step size: 0.02° 2θ à 10 s counting time). Quantitative phase analysis was accomplished performing Rietveld analysis with the software BGMN 4.2.3 (Taut et al., 1998).

Thin sections were produced from three "active arkose" samples and studied microscopically before selecting two of them for laser-ablation (NewWave UP193Fx, ArF-Excimer-Laser) ICP-MS (PerkinElmer Elan DRCe) analysis (calibration standard: NIST 612, spot diameter: 150 µm) to characterize major and trace element abundance and distribution on a microscale.

Eight samples (five "active arkoses", two sandstones, one clay band) were subjected to a sequential extraction procedure (SEP). The BCR approach (Ure et al., 1993) was used as a basis. It was modified after Sahuquillo et al. (1999) to improve method reproducibility. Moreover, an extraction step targeting the trace element fraction bound to apatite after Nezat et al. (2007) was added to the procedure. These authors found that 1 M HNO_3 congruently dissolves apatite at 20° C but that the solution becomes saturated at ~90 mmol

apatite L^{-1}. Converting this finding to 10 mL solution (needed to work with 1 g solid sample and the solid-solution ratio 1:10 used by Nezat et al. (2007), ~0.44 g of apatite are dissolvable. According to the geochemical and mineralogical results in this study, up to 0.5 g apatite g^{-1} solid sample can be expected (cf. 3.2). The solid-solution ratio for this step was therefore changed to 1:20. Aliquots of the samples (1 g) were ground in an agate mortar and placed in 50 mL centrifugation tubes. Extraction solutions were added in each step and the respective procedure was carried out. After centrifugation (15 min, 3000 rpm) and filtration (0.45 µm cellulose acetate filters) of the supernatant solution, a washing step with 20 mL deionized water (15 min shaking, 15 min centrifugation, supernatant discarded) was implemented to avoid U transfer to the next fraction. Subsequently, the remaining sediment was subjected to the following procedure (Table 1). Extracted solutions were analyzed for U using ICP-MS (PerkinElmer Elan DRCe).

Step no.	Target U fraction	Extractant	Procedure
1	Easily mobilizable	CH_3COOH (0.11 M)	16 h shaking, 20°C
2	Reducible	NH_2OH-HCl (0.5 M)	16 h shaking, 20°C
3	Oxidizable	H_2O_2 (30 %)	2 h in a water bath (85°C)
4	Bound to apatite	HNO_3 (1 M)	16 h shaking, 20°C
5	Residual	$U_{tot} - U_{\sum steps\ 1\text{-}4}$	

Table 1. Applied sequential extraction procedure ("BCR+apatite").

3 Results and Discussion

3.1 Uranium distribution in drinking water

The distribution of U in Bavarian drinking water (Fig. 1) documents U "hot spots" around Nürnberg and Bamberg with a maximum U concentration of about 40 µg L^{-1}, and rather unremarkable values (<10 µg L^{-1}) in the southern and eastern parts of the federal state. There is a marked congruence of this spatial groundwater U pattern with the facies distribution of U-rich phoscretes ("active arkoses") and dolcretes (Fig. 1,3) in the "Burgsandstein" aquifer, which gives a first indication towards a geological U source in the area.

3.2 Aquifer geochemistry and mineralogy

While aquifer sandstones exhibit low median U contents of 1.3 µg g^{-1}, embedded "active arkoses" contain up to 260 µg g^{-1} U in bulk rock samples. Their median enrichment factors

compared to the sandstones are 44 for U, 32 for Ca and 98 for P. They furthermore represent sinks for Fe, most REE, Y, V, Pb and Cr while other minor and trace elements are in equal range or even depleted (Fig. 4, see complete data table A2 in the Appendix).

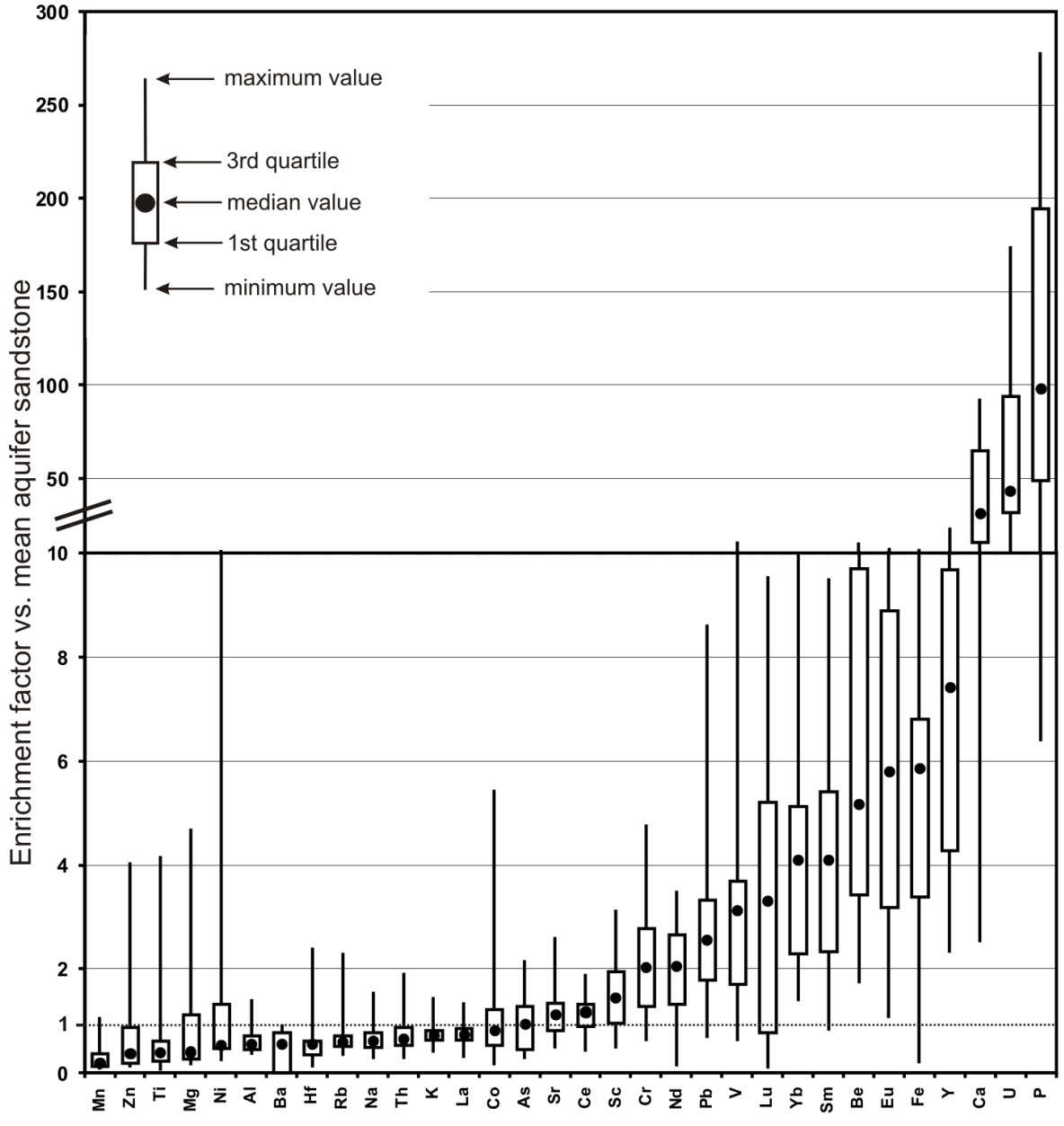

Fig. 4. Element enrichment/depletion of "active arkoses" compared to mean aquifer sandstone concentrations, ordered by increasing median of enrichment factors. Note change of scale on the ordinate.

Quantitative XRD analyses indicate the aquifer sandstone is composed of dominantly quartz (nearly 90 wt.%) with minor amounts of feldspars and clay minerals. "Active arkoses" contain varying degrees of quartz (24-81 wt.%), feldspars (6-17 wt.%) and clay minerals (1-18 wt.%). Fluorapatite is always present, sometimes as a dominant component up to 50 wt.%. The relatively high Fe content is present as hematite (1-11 wt.%) and Fe-bearing clay minerals like chlorite and illite (Table 2).

	Quartz	Feldspars	Clay minerals	F-Apatite	Hematite
	wt.%	wt.%	wt.%	wt.%	wt.%
Sandstones					
Sand_1	87	6.4	6.3	n.d.	n.d.
Sand_2	89	7.3	3.6	n.d.	n.d.
Clay band					
Clay_1	21	16	59	n.d.	2.9
"Active arkoses"					
AA_1_inner core	59	17	18	0.9	5.2
AA_1_outer core	24	6.2	9.3	50	11
AA_1_purple rim	74	9.8	6.0	9.5	0.5
AA_2	69	8.5	0.8	20	2.1
AA_3	68	13	3.6	12	4.6
AA_4	81	6.3	1.2	9.9	1.4
AA_5	81	10	2.3	1.9	4.5

Table 2. Results of quantitative XRD analyses. "Feldspars" – sum of orthoclase and microcline, "Clay minerals" – sum of kaolinite, illite and chlorite. "n.d." – not detected. Cf. 3.3 for "AA_1" details.

Plotting the bulk contents of the main apatite components Ca and P in "active arkoses" yields a very close positive correlation (R^2>0.99, Fig. 5) and enables the calculation of F and CO_2 concentrations in the minerals – 3.9 and 4.5 wt.%, respectively. Thus, a comparison to stoichiometric fluorapatite in terms of Ca:P ratio documents a clear offset caused by partial coupled substitution of $CO_3^{2-} + F^-$ for PO_4^{3-} in the crystal structure (Binder and Troll, 1989; Regnier et al., 1994). This suggests a francolite stoichiometry close to $Ca_5(PO_4)_{2.5}(CO_3)_{0.5}F_{1.5}$ in the studied samples.

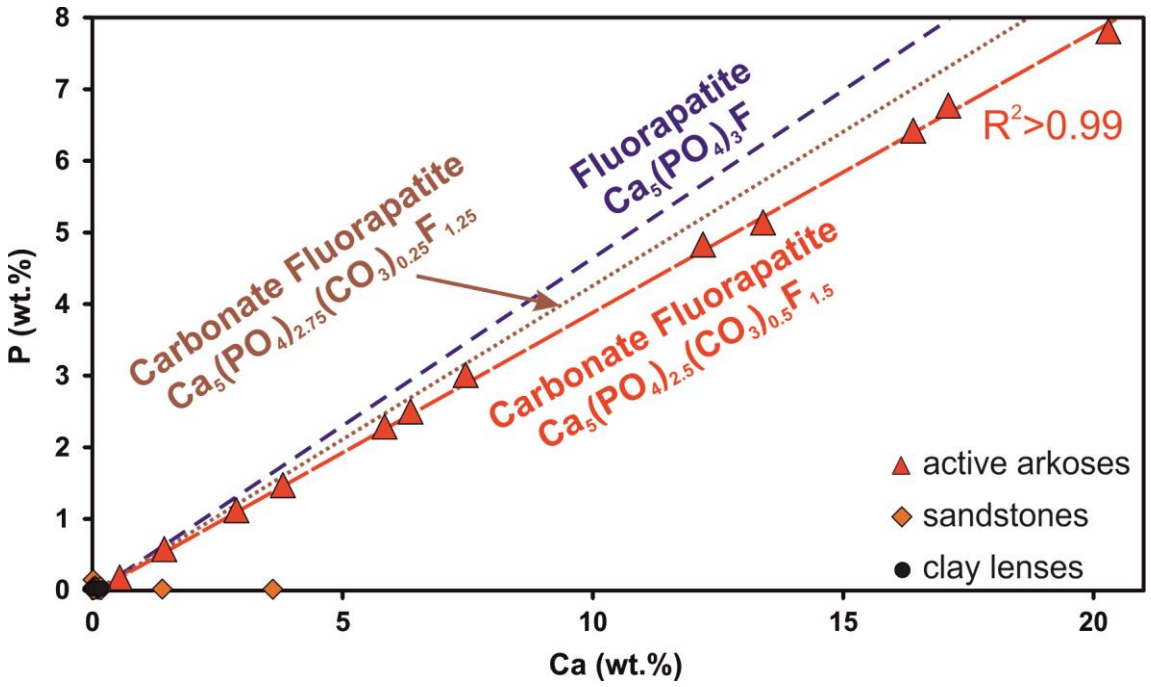

Fig. 5. Ca-P scatter plot for studied sediments. Lines for ideal fluorapatite stoichiometries with different degrees of carbonate substitution for phosphate are indicated (equivalent to 0 wt.% [blue line], 2.25 wt.% [brown line] and 4.5 wt.% [red line] structural CO_2). The studied francolites plot exactly along the $Ca_5(PO_4)_{2.5}(CO_3)_{0.5}F_{1.5}$ stoichiometry. Aquifer sandstones and interbedded clay lenses do not show indications for apatite presence.

XRD results for unit cell parameters were used to evaluate the substitutional effect on the apatite crystal structure by comparing to values for Cl-, OH- and F-apatite end members and a carbonate fluorapatite (Table 3).

	$Ca_5(PO_4)_3Cl$	$Ca_5(PO_4)_3OH$	$Ca_5(PO_4)_3F$	Carb-F	this study
a (Å)	9.5979[a]	9.4166[a]	9.3973[a]	9.368±0.002[b]	9.364±0.003
Offset from apatites in this study (Å)	+0.234	+0.053	+0.033	+0.004	
c (Å)	6.7762[a]	6.8745[a]	6.8782[a]	6.890±0.002[b]	6.895±0.005
Offset from apatites in this study (Å)	-0.119	-0.021	-0.017	-0.005	

Table 3. Apatite unit cell parameters in comparison to end members of the $Ca_5(PO_4)_3(Cl,OH,F)$ structure and carbonate fluorapatite (Carb-F). [a]data from Hughes et al., 1989; [b]data from Gulbrandsen et al., 1966.

Cell dimensions of the studied apatites are almost identical with the carbonate fluorapatite (Table 3). Substitution of planar CO_3^{2-} for tetrahedral PO_4^{3-}, accompanied by occupation of the vacant oxygen site by F^-, can cause significant changes in the crystal structure, expressed by changes in unit cell parameters. This includes shortening of the a-axis and elongation of the c-axis, compared to apatite end members (Smith and Lehr, 1966), as is observed in our samples. Consequently, apatites analyzed in this study are characterized as francolites containing high amounts of structural CO_2 – especially when considering that the maximum CO_3^{2-} substitution until disruption of the francolite structure corresponds to 6.3 wt.% CO_2 (McArthur, 1985).

3.3 Microscale U distribution

LA-ICP-MS measurements were conducted to characterize the distribution of U and other elements on a microscale. A bulb-like active arkose with distinct zonation, sampled from a fresh outcrop, was selected for chemical profiling and microscopical characterization (Fig. 6).

The reddish inner core of the sample contains little apatite (0.9 wt.%) and low U (mean: 25 µg g^{-1}), but high Fe contents (mean: 18 wt.%). Conversely, the thicker purple outer core reaches 50 wt.% fluorapatite and U of about 400 µg g^{-1} with several concentration peaks of up to 1070 µg g^{-1}. The latter are observed in relatively pure, grey apatite matrix bands (high Ca and P, low Fe) visible under the microscope and probably formed by accretive crystallization of francolite (Fig. 6). Uranium hosting by apatite – not hematite – is confirmed here. Significantly lower elemental contents were detected in the yellow/white "leached" rim of the "active arkose". Single reddish matrix spots with higher concentrations probably represent relics of a formerly more abundant material. This indicates a past mobilization mechanism and, therefore, U release to solution in the course of water-rock-interaction processes.

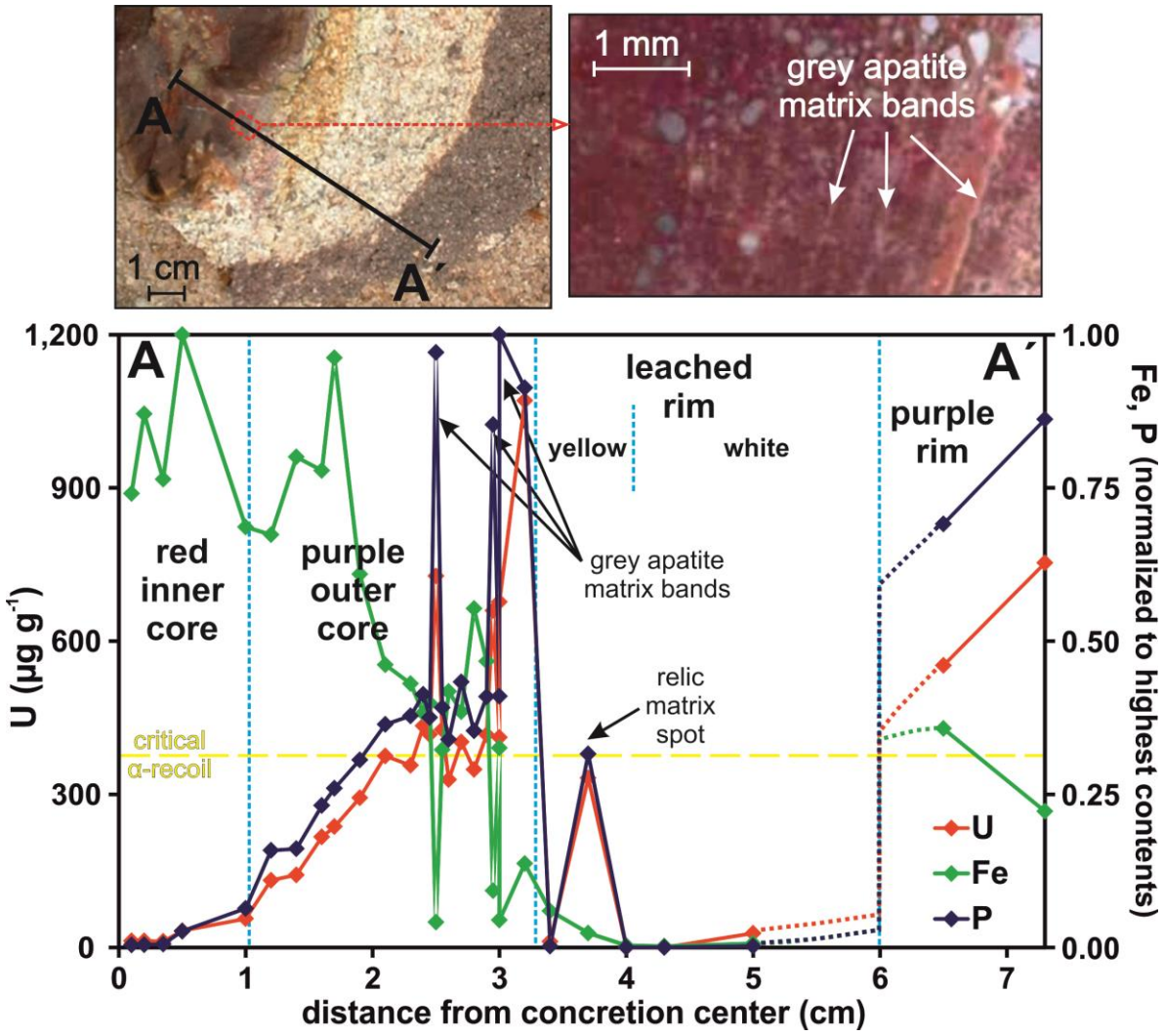

Fig. 6. LA-ICP-MS data for U, Fe and P along a zoned active arkose sample profile (A-A´). The line of calculated critical α-recoil damage in apatite (at 370 µg g^{-1} U) is indicated (cf. 3.4). Vertical dashed blue lines mark zone boundaries of the active arkose specimen (cf. 3.3).

3.4 Uranium fractionation and remobilization

Mineralogical fractionation and remobilization behaviour of U were assessed in a sequential extraction procedure (SEP). Easily mobilizable, i.e. CH_3COOH-extractable, U represents 7 % of the total U pool in active arkoses on average. However, a freshly exposed specimen yielded no more than 1 % U_{tot} in this fraction. Thus, secondary alteration is likely to lead to U oxidation and transformation into more soluble species, suggesting elevated U mobility in active arkoses during weathering. Uranium concentrations in the apatite-targeting extraction step (1 M HNO_3) are highly variable in active arkoses (<1 to >80 %

U_{tot}). Specifically, 294 µg g^{-1} U were dissolved from a freshly exposed francolite-rich specimen. Samples from older, more weathered outcrops follow a trend towards lower apatite content and simultaneously decreasing U dissolution by HNO_3 (Fig. 7).

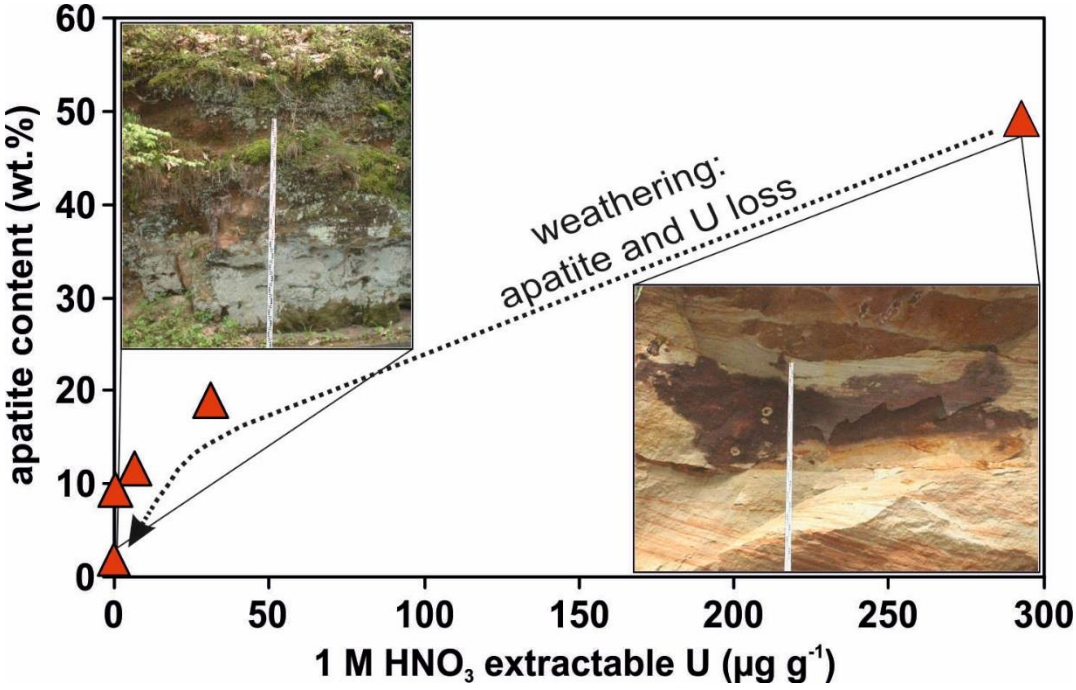

Fig. 7. Apatite-hosted U concentration (determined by 1 M HNO_3 extraction) vs. apatite content (determined by quantitative XRD) in active arkoses from very fresh (right picture) and weathered (left picture) outcrops.

Negligible U mobilization was detected for samples with less than 10 wt.% fluorapatite although they partly contain significant bulk U concentrations (cf. Appendix A2), largely bound in the unreactive residual fraction as determined by SEP (cf. Table 1). It is concluded that the aforementioned trend represents a weathering line (i.e. a geochemical development from the upper right to the lower left corner in Fig. 7 during weathering) including a gradual loss of apatite and a decreasing reactivity in terms of U mobilization potential.

At first glance, these results appear surprising given the generally low solubility of fluorapatite ($K_{s0} = 10^{-60.6}$; Valsami-Jones et al., 1998). Nevertheless, apatite was shown to be the least stable member of the heavy mineral group (Lång, 2000) – its weathering is considered to control P fluxes and availability in the exosphere, and thus biological productivity on geological time scales (Guidry and Mackenzie, 2000). Solubility and vulnerability to weathering and thus, trace element mobilization potential, of the francolites studied here are likely to be significantly enhanced compared to standard apatites in laboratory studies, mainly for two reasons. Firstly, fluorapatite structural stability is significantly altered by coupled CO_3^{2-} substitution – mineral solubility increases dramatically with increasing carbonate content (Jahnke, 1984). This effect is due to the

interstitial position of substituted F^- ions in the mineral structure and associated breakdown of crystal symmetry, already at 1 wt.% structural CO_2 in the apatite (Regnier et al., 1994). Secondly, radiation from U decay in certain minerals of sufficient U concentration and/or age can greatly increase dissolution rates due to α-recoil damage in the crystals. A critical dose of radiation must be exceeded in order to drastically enhance mineral solubility in an aqueous solution of typical groundwater composition. Apatite is sensitive to radiation-enhanced dissolution, whereas e.g.uraninite and zircon do not show this effect (Petit et al., 1985). Uranium concentrations necessary to reach a critical dose of α-recoil damage were calculated for the studied francolite using equation (1) (Petit et al., 1985).

(1) $N_c = T * n_i * \lambda_i * C_i$

where

N_c is the critical dose of α-recoil [cm^{-3}]

T is the mineral age [a]

n_i is the number of α-decays in the disintegration chain of a radioactive element [-]

λ_i is the decay constant of the radioactive element [a^{-1}]

C_i is the concentration of the radioactive element in the mineral [atoms g^{-1}]

Calculations were only performed for U as it is the only relevant radioactive component in the analyzed francolites, Th radiation is negligible (Abele et al., 1962). Ergo, $n_i = 8$ and $\lambda_i = 1.53 * 10^{-10}\ a^{-1}$. N_c is given as $2.5 * 10^{18}\ cm^{-3}$ (Petit et al., 1985), T was set to 210 Ma accounting for the syngenetic formation of the francolites in Norian times. It is then possible to calculate the minimum U concentration necessary to exceed the critical α-decay dose reached after mineral formation, and to evaluate if francolite U contents are sufficient to account for significantly radiation-enhanced solubility. With a carbonate fluorapatite density of 3.12 g cm^{-3} (Barthelmy, 2011), the result of the calculation is ca. 370 µg g^{-1} U. Regarding U concentrations in the studied apatites of up to 1070 µg g^{-1} (cf. 3.3), it is concluded that a high percentage of the Norian francolites clearly exceed the critical dose value and thus exhibit radiation-enhanced solubility and an increased tendency to lose incorporated U to solution and, therefore, to groundwater of the study area.

4 Conclusions

In groundwater extracted from an important Upper Triassic sandstone aquifer ("Burgsandstein") in Northern Bavaria, elevated concentrations of U, partly in excess of the drinking water limitation, were identified in recent years. The geological conditions probably responsible for the creation of this hydrochemical signature are discussed here. Results indicate the major role of abundant syngenetic intercalations within the terrestrial

facies of the aquifer sandstones, so-called "active arkoses". These exhibit a carbonate fluorapatite (francolite)-dominated matrix containing high U contents hosted by the francolite. It was shown here that the studied francolite is highly susceptible to alteration and thus, loss of the heavy metal to solution. In consequence, active arkoses were identified as most likely source for elevated groundwater U in the study area – their weathering controls the geogenic U problem in Northern Bavaria.

This study tried to shed light not only on the background of Germany´s most significant groundwater U problem area, but also on the probably underestimated importance of the ubiquitary apatite mineral family members as players in the structure of trace element sources and sinks in many affected areas worldwide. This appears to be especially true for U, an element which increasingly finds itself in the focus of hydrogeochemical and health-related research.

Acknowledgements

The Institute of Clay and Interface Mineralogy (CIM, RWTH Aachen University) is acknowledged for enabling mineralogical analyses. The authors thank the Bavarian Environment Agency (LfU) for assistance in field work planning, hydrochemical data and discussions.

References

Abele G., Berger K., Salger M. (1962) Die Uranvorkommen im Burgsandstein Mittelfrankens. *Geol. Bavar.* **19**, 3-90.

Baborowski M., Bozau E. (2006) Impact of former mining activities on the uranium distribution in the river Saale (Germany). *Appl. Geochem.* **21**, 1073-1082.

Banning A., Cardona A., Rüde T. R. (2012) Uranium and arsenic dynamics in volcano-sedimentary basins – an exemplary study in north-central Mexico. *Appl. Geochem.* **27**, 2160-2172.

Banning A., Demmel T., Rüde T. R., Wrobel M. (2013) Groundwater uranium origin and fate control in a river valley aquifer. *Environ. Sci. Technol.* **47**, 13941-13948.

Barthelmy D. (2011) Carbonate-fluorapatite mineral data. http://webmineral.com/data/Carbonate-fluorapatite.shtml

Binder G., Troll G. (1989) Coupled anion substitution in natural carbon-bearing apatites. *Contrib. Mineral. Petr.* **101**, 394-401.

Carvalho I. G., Cidu R., Fanfani L., Pitsch H., Beaucaire C., Zuddas P. (2005) Environmental impact of uranium mining and ore processing in the Lagoa Real district, Bahia, Brazil. *Environ. Sci. Technol.* **39**, 8646-8652.

Crançon P., Pili E., Charlet L. (2010) Uranium facilitated transport by water-dispersible colloids in field and soil columns. *Sci. Total Environ.* **408**, 2118-2128.

382 Dahanayake K., Subasinghe S. M. N. D. (1989) Secondary phosphate mineralization in a
383 karstic environment in central Sri Lanka. *Miner. Deposita* **24**, 169-175.

384 Dill H. G. (1988) Diagenetic and epigenetic U, Ba, and base metal mineralization in the
385 arenaceous Upper Triassic "Burgsandstein", southern Germany. *Miner. Petrol.* **39**,
386 93-105.

387 Dill H. G. (2010) Authigenic heavy minerals a clue to unravel supergene and hypogene
388 alteration of marine and continental sediments of Triassic to Cretaceous age (SE
389 Germany). *Sediment. Geol.* **228**, 61-76.

390 Dong W., Xie G., Miller T. R., Franklin M. P., Palmateer Oxenberg T., Bouwer E. J., Ball
391 W. P., Halden R. U. (2006) Sorption and bioreduction of hexavalent uranium at a
392 military facility by the Chesapeake Bay. *Environ. Pollut.* **142**, 132-142.

393 Foodwatch (2008) Bayern: Uran im Trinkwasser, Stand: 03.04.2008 [Bavaria:
394 Uranium in drinking water, status: april 3, 2008]. http://www.foodwatch.org/fileadm
395 in/Themen/Uran/Dokumente/Uranwerte_2008_Bundeslaender/20080403_foodwatc
396 h_bayern_uran_wasser_durchsuchbar.pdf

397 Frengstad B., Skrede A. K. M., Banks D., Krog J. R., Siewers U. (2000) The chemistry of
398 Norwegian groundwaters: III. The distribution of trace elements in 476 crystalline
399 bedrock groundwaters, as analysed by ICP-MS techniques. *Sci. Total Environ.* **246**,
400 21-40.

401 Guidry M. W., Mackenzie F. T. (2000) Apatite weathering and the Phanerozoic phosphorus
402 cycle. *Geology* **28**, 631-634.

403 Gulbrandsen R. A., Kramer J. R., Beatty L. B., Mays R. E. (1966) Carbonate-bearing
404 apatite from Faraday township, Ontario, Canada. *Am. Mineral.* **51**, 819-824.

405 Heinrichs G., Udluft P. (1999) Natural arsenic in Triassic rocks: a source of drinking water
406 contamination in Bavaria, Germany. *Hydrogeol. J.* **7**, 468-476.

407 Hughes J. M., Cameron M., Crowley K. D. (1989) Structural variations in natural F, OH,
408 and Cl apatites. *Am. Mineral.* **74**, 870-876.

409 Jahnke R. A. (1984) The synthesis and solubility of carbonate fluorapatite. *Am. J. Sci.* **284**,
410 58-78.

411 Kurttio P., Harmoinen A., Saha H., Salonen L., Karpas Z., Komulainen H., Auvinen A.
412 (2006) Kidney toxicity of ingested uranium from drinking water. *Am. J. Kidney Dis.*
413 **47**, 972-982.

414 Lång L.-O. (2000) Heavy mineral weathering under acidic soil conditions. *Appl. Geochem.*
415 **15**, 415-423.

416 McArthur J. M. (1985) Francolite geochemistry – compositional controls during formation,
417 diagenesis, metamorphism and weathering. *Geochim. Cosmochim. Acta* **49**, 23-35.

418 Nezat C. A., Blum J. D., Yanai R. D., Hamburg S. P. (2007) A sequential extraction to
419 determine the distribution of apatite in granitoid soil mineral pools with application

to weathering at the Hubbard Brook Experimental Forest, NH, USA. *Appl. Geochem*. **22**, 2406-2421.

Petit J.-C., Langevin Y., Dran J.-C. (1985) Radiation-enhanced release of uranium from accessory minerals in crystalline rocks. *Geochim. Cosmochim. Acta* **49**, 871-876.

Rakovan J., Reeder R. J., Elzinga E. J., Cherniak D. J., Tait C. D., Morris D.E. (2002) Structural characterization of U(VI) in apatite by X-ray absorption spectroscopy. *Environ. Sci. Technol.* **36**, 3114-3117.

Read D., Bennett D. G., Hooker P. J., Ivanovich M., Longworth G., Milodowski A. E., Noy D. J. (1993) The migration of uranium into peat-rich soils at Broubster, Caithness, Scotland, U.K. *J. Contam. Hydrol.* **13**, 291-308.

Regnier P., Lasaga A. C., Berner R. A., Han O. H., Zilm K. W. (1994) Mechanism of CO_3^{2-} substitution in carbonate-fluorapatite: evidence from FTIR spectroscopy, 13C NMR, and quantum mechanical calculations. *Am. Mineral.* **79**, 809-818.

Sahuquillo A., López-Sánchez J. F., Rubio R., Rauret G., Thomas R. P., Davidson C. M., Ure A. M. (1999) Use of a certified reference material for extractable trace metals to assess sources of uncertainty in the BCR three-stage sequential extraction procedure. *Anal. Chim. Acta* **382**, 317-327.

Schnug E., Lottermoser B. G. (2013) Fertilizer-derived uranium and its threat to human health. *Environ. Sci. Technol.* **47**, 2433−2434.

Smith J. P., Lehr J. R. (1966) An X-ray investigation of carbonate apatites. *J. Agr. Food Chem*. **14**, 342-349.

Starinsky A., Katz A., Kolodny Y. (1982) The incorporation of uranium into diagenetic phosphorite. *Geochim. Cosmochim. Acta* **46**, 1365-1374.

Swirydczuk K., Wilkinson B. H., Smith G. R. (1981) Synsedimentary lacustrine phosphorites from the Pliocene Glenns Ferry Formation of Southwestern Idaho. *J. Sediment. Res.* **51**, 1205-1214.

Taut T., Kleeberg R., Bergmann J. (1998) The new Seifert Rietveld program BGMN and its application to quantitative phase analysis. *Mater. Struct*. **5**, 57-66.

Ure A. M., Quevauviller P., Muntau H., Griepink B. (1993) Speciation of heavy metals in soils and sediments. An account of the improvement and harmonization of extraction techniques undertaken under the auspices of the BCR of the Commission of the European Communities. *Int. J. Environ. An. Ch.* **51**, 135-151.

Valsami-Jones E., Ragnarsdottir K. V., Putnis A., Bosbach D., Kemp A. J., Cressey G. (1998) The dissolution of apatite in the presence of aqueous metal cations at pH 2-7. *Chem. Geol.* **151**, 215-233.

Zamora M. L., Tracy B. L., Zielinski J. M., Meyerhof D. P., Moss M. A. (1998) Chronic ingestion of uranium in drinking water: a study of kidney bioeffects in humans. *Toxicol. Sci.* **43**, 68-77.

Zielinski R. A., Orem W. H., Simmons K. R., Bohlen P. J. (2006) Fertilizer-derived uranium and sulphur in rangeland soil and runoff: a case study in central Florida. *Water Air Soil Poll.* **176**, 163-183.

490 **Figure captions**

491

492 **Fig. 1.** Uranium concentrations in Bavarian drinking water and distribution of uraniferous
493 facies in Triassic sandstones (the latter after Dill, 1988). The dashed red box indicates the
494 study area.

495 **Fig. 2.** Keuper stratigraphy of the study area with sampled units highlighted by hachures,
496 approximate unit thicknesses and basic hydrogeology (modified after Heinrichs and Udluft,
497 1999). "Active arkoses" only occur in Middle and Upper "Burgsandstein" aquifers, parts of
498 the terrestrial Norian "Sandsteinkeuper".

499 **Fig. 3.** Paleogeographical situation during the Middle Keuper with sediment input
500 directions, sediment thicknesses and distribution of the main U-bearing depositional facies
501 (modified after Dill, 1988; Dill 2010). See Fig. 1 for a geographical overview. The
502 sedimentary basin filling mainly derived from erosion of the Vindelician Swell – a former
503 part of the Central European Variscides consisting of crystalline magmatic and
504 metamorphic rocks – under arid conditions. It may be subdivided into a terrestrial (alluvial
505 fan with playa lakes) and a basinal (shallow marine) facies with transitional character
506 (sabhka) in between (Abele et al., 1962; Dill, 2010; Heinrichs and Udluft, 1999).

507 **Fig. 4.** Element enrichment/depletion of "active arkoses" compared to mean aquifer
508 sandstone concentrations, ordered by increasing median of enrichment factors. Mind
509 change of scale on the ordinate.

510 **Fig. 5.** Ca-P scatter plot for studied sediments. Lines for ideal fluorapatite stoichiometries
511 with different degrees of carbonate substitution for phosphate are indicated (equivalent to
512 0 wt.% [blue line], 2.25 wt.% [brown line] and 4.5 wt.% [red line] structural CO_2). The
513 studied francolites plot exactly along the $Ca_5(PO_4)_{2.5}(CO_3)_{0.5}F_{1.5}$ stoichiometry. Aquifer
514 sandstones and interbedded clay lenses do not show indications for apatite presence.

515 **Fig. 6.** LA-ICP-MS data for U, Fe and P along a zoned "active arkose" sample profile (A-
516 A´). The line of calculated critical α-recoil damage in apatite (at 370 µg g^{-1} U) is indicated
517 (cf. 3.4). Vertical dashed blue lines mark zone boundaries of the active arkose specimen (cf.
518 3.3).

519 **Fig. 7.** Apatite-hosted U concentration (determined by 1 M HNO_3 extraction) vs. apatite
520 content (determined by quantitative XRD) in "active arkoses" from very fresh (right
521 picture) and weathered (left picture) outcrops.